

Ternary compound HfCuP: An excellent Weyl semimetal with the coexistence of type-I and type-II Weyl nodes



Weizhen Meng^a, Xiaoming Zhang^{a,b,*}, Tingli He^a, Lei Jin^a, Xuefang Dai^a, Ying Liu^a, Guodong Liu^{a,b,c,*}

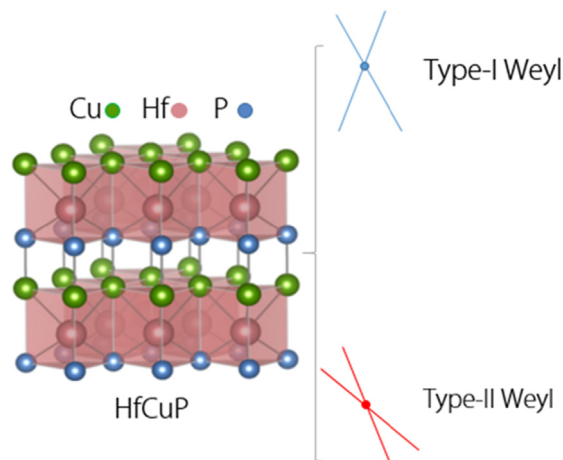
^a School of Materials Science and Engineering, Hebei University of Technology, Tianjin 300130, China

^b State Key Laboratory of Reliability and Intelligence of Electrical Equipment, Hebei University of Technology, Tianjin 300130, China

^c School of Physics and Electronic Engineering, Chongqing Normal University, Chongqing 400044, China

GRAPHICAL ABSTRACT

Ternary compound HfCuP is a potential Weyl semimetal coexisting both type-I and type-II Weyl nodes.



ARTICLE INFO

Article history:

Received 6 March 2020

Revised 26 May 2020

Accepted 31 May 2020

Available online 4 June 2020

Keywords:

Topological materials

Weyl semimetals

ABSTRACT

In most Weyl semimetal (WSMs), the Weyl nodes with opposite chiralities usually have the same type of band dispersions (either type-I or type-II), whereas realistic candidate materials hosting different types of Weyl nodes have not been identified to date. Here we report for the first time that, a ternary compound HfCuP, is an excellent WSM with the coexistence of type-I and type-II Weyl nodes. Our results show that, HfCuP totally contains six pairs of type-I and six pairs of type-II Weyl nodes in the Brillouin zone, all locating at the H-K path. These Weyl nodes situate slightly below the Fermi level, and do not coexist with other extraneous bands. The nontrivial band structure in HfCuP produces clear Fermi arc surface states in the (1 0 0) surface projection. Moreover, we find the Weyl nodes in HfCuP can be effectively tuned by

Peer review under responsibility of Cairo University.

* Corresponding author.

E-mail addresses: zhangxiaoming87@hebut.edu.cn (X. Zhang), gdlu1978@126.com (G. Liu).

<https://doi.org/10.1016/j.jare.2020.05.026>

2090-1232/© 2020 THE AUTHORS. Published by Elsevier BV on behalf of Cairo University.

This is an open access article under the CC BY-NC-ND license (<http://creativecommons.org/licenses/by-nc-nd/4.0/>).

Fermi arc
First principles

strain engineering. These characteristics make HfCuP a potential candidate material to investigate the novel properties of type-I and type-II Weyl fermions, as well as the potential entanglements between them.

© 2020 THE AUTHORS. Published by Elsevier BV on behalf of Cairo University. This is an open access article under the CC BY-NC-ND license (<http://creativecommons.org/licenses/by-nc-nd/4.0/>).

Introduction

Since the theoretical discovery and experimental realization of topological insulators [1–3], topological aspects of matter have received intense research interests. Recently, such nontrivial band topology has been further extended to semi-metallic/metallic systems, giving rise to various categories of topological semimetals/metals such as Dirac, Weyl, nodal line, and nodal surface semimetals [4–28]. These topological materials have shown a wide range of potential applications including electronics, biosensing, catalysis, optoelectronics, superconductivity, and so on [29–37]. Among topological materials, Weyl semimetals (WSMs) have received particular attention because the band crossing at the Weyl nodes have the minimum (twofold) band degeneracy [4,10,13], which greatly facilitates the understanding of the fundamental band topology. In WSMs, the Weyl nodes appear in pairs with the opposite chirality [10,38,39]. As the results, some novel phenomena such as negative magnetoresistivity and anomalous Hall effects are observed in WSMs [40–44]. In the momentum space, the Weyl cone can be tilted. This produces the classification of WSMs into the type-I and type-II WSMs. Type-I WSMs have conventional conical band dispersions [10–13,45,46], which follow the Lorentz symmetry. However, in type-II WSMs, the Weyl cones are completely tilted, which can lead to the contact of hole-like and electron-like states at the same energy level [47–49]. Type-II WSMs are proposed to host distinct properties from type-I WSMs, which include modified anomalous Hall conductivity, direction-dependent chiral anomaly, and momentum space Klein tunneling [50–53].

Up to now, many WSMs have been proposed in realistic materials. The TaAs family, as the representative example for type-I WSMs, has been well studied both theoretically and experimentally [10,13,45]. Type-II WSMs have also been realized in many existing materials including $\text{Mo}_x\text{W}_{1-x}\text{Te}_2$ ($x = 0-1$), Ta_3S_2 and LaAlGe [47,54,55]. For these examples, however, the Weyl nodes with opposite chiralities are either type-I or type-II, i.e., they have the same type of band dispersion. Obviously, WSMs which host both type-I and type-II Weyl nodes simultaneously can represent another distinct category. In this category of WSMs, all the intriguing properties for both type-I and type-II Weyl nodes can happen in one material. Meanwhile, they also provide a good platform to investigate potential entanglement between Weyl nodes with different types of band dispersions. Under such consideration, Li et al. first construct a hybrid WSM with coexisting type-I and type-II Weyl nodes by using the tight-binding model [56]. Later, also in the Hamiltonian model scale, Xie et al. propose that disorder can introduce phase transition from type-I to type-II in WSMs [57]. Quite recently, Zhang et al. reported that the material OsC_2 can host 24 type-I Weyl nodes and 12 type-II Weyl nodes in the native state [58]. Unfortunately, OsC_2 is a hypothetical material and has not been synthesized in experiments [59]. Therefore, it is in great significance to develop realistic WSMs containing both type-I and type-II Weyl nodes simultaneously.

In this work, we report that a ternary compound namely HfCuP is also such WSM, which exhibits novel band structure with the coexistence of type-I and type-II Weyl nodes. It is found that HfCuP totally contains six pairs of type-I and six pairs of type-II Weyl nodes, situating at both sides of the H point in the H-K path. First principles calculations have located the positions for all the Weyl

nodes, and the corresponding Fermi arc surface states are identified. Very importantly, the Weyl nodes in HfCuP are quite close to the Fermi level without coexisting with extraneous bands nearby, which greatly favors their detection in experiments. We constructed the effective Hamiltonian for the Weyl nodes, which can well describe the quasiparticle excitations near the Weyl node. In addition, we find the band topology in HfCuP can be tuned by strain engineering, making the Weyl nodes in HfCuP controllable.

Crystal structure of HfCuP

Ternary compound HfCuP crystallizes in a trigonal structure with the $P3m1$ space group (No. 156). As shown in Fig. 1(a), surrounded by three Cu atoms and three P atoms, Hf atom is bonded in the six-coordinate geometry. Meanwhile, each P atom bonds with two Hf atoms and one Cu atom, forming the tetrahedral local structure. As shown in Fig. 1(b), the HfCuP primitive cell contains three atoms, where Hf, Cu and P atoms occupy the (0, 0, 0.998), (1/3, 2/3, 0.634) and (1/3, 2/3, 0.224) Wyckoff sites, respectively. The ternary compound HfCuP was firstly prepared in 2005 [60], and its crystal structure was also provided in the Materials Project [61].

Results and discussions

Fig. 2(a) shows the band structure of HfCuP without considering spin-orbit coupling (SOC). For computational details, please see the Supplementary Information. It takes on a clear semimetallic band structure, where a band crossing happens in the H-K path near the Fermi level. Besides the band crossing, the conduction band and valence band are well separated with each other in other high-symmetry paths. After examining the projected density of

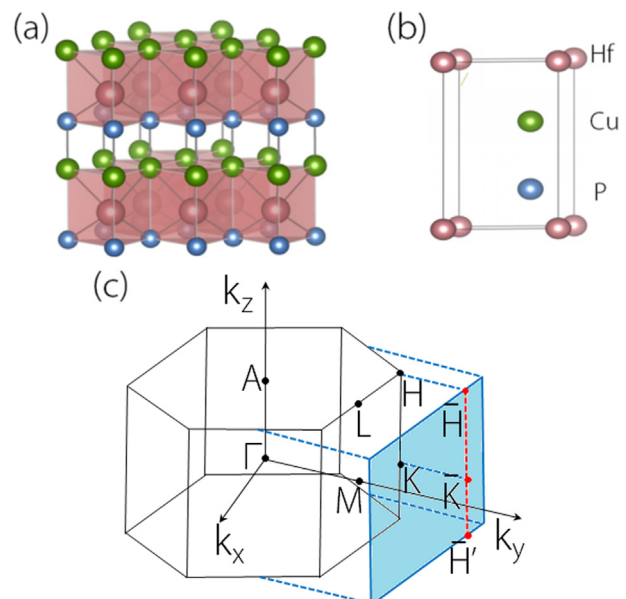


Fig. 1. (a) Crystal structure and (b) the primitive cell of HfCuP. (c) The bulk and the (1 0 0) surface Brillouin zone of HfCuP.

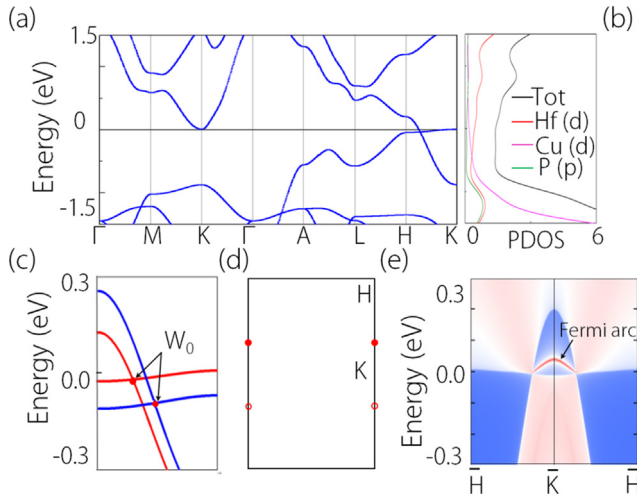


Fig. 2. (a) Electronic band structure of HfCuP without considering SOC. (b) The projected density of states (PDOS) of HfCuP. (c) The enlarged band structure of HfCuP along the H-K path. The blue and red bands in (c) are calculated from PBE and HSE06, respectively. (d) The position of W_0 in the (1 0 0) surface. In (d), the solid and hollow circles represent the “positive” and “negative” Weyl nodes. (e) The (1 0 0) surface band structure of HfCuP. In (c), the arrow points the Fermi arc surface states. (For interpretation of the references to colour in this figure legend, the reader is referred to the web version of this article.)

states of HfCuP, we find the states near the Fermi level are almost contributed by the 5d orbitals of Hf atoms [see Fig. 2(b)]. By performing symmetry analysis, we find the two crossing bands correspond to the E and E^* irreducible representations of the C_3 symmetry in the H-K path. Since both bands are singlet, the crossing point is in fact a Weyl node (denoted as W_0). The enlarged band structure near W_0 is shown in Fig. 2(c). More careful calculations show that W_0 locates at (0.333, 0.667, ± 0.150) in the Brillouin zone (BZ), situating at 33 meV below the Fermi level. Considering the PBE functional usually underestimates the potential band gap, we recheck the band structure near W_0 under the hybrid HSE06 functional. We find the Weyl node retains in the H-K path, although its position experiences a slight change [see Fig. 2(c)]. Considering the lattice symmetry, there in fact contains six pairs of such Weyl nodes in HfCuP, situating at both sides of the H point in the H-K path. The positions of the Weyl nodes in the (1 0 0) surface projection are shown in Fig. 2(d).

Let us consider the space group 156, which can host a Weyl point along H-K path. This path is an invariant subspace of C_{3z} . Since $[C_{3z}, H(\mathbf{k})] = 0$, the Bloch states in this path can be chosen as the eigenstates of C_{3z} . We denote the Bloch states with $\{|c_{3z}\rangle\}$ with $c_{3z} \in \{e^{i\frac{2\pi}{3}}, e^{-i\frac{2\pi}{3}}\}$ the eigenvalues of C_{3z} . The matrix representation of the operator can be expressed in the above basis as,

$$C_3 = \begin{bmatrix} e^{i\frac{2\pi}{3}} & 0 \\ 0 & e^{-i\frac{2\pi}{3}} \end{bmatrix} \quad (1)$$

The effective Hamiltonian is required to be invariant under this operator, such that

$$C_{3z}H(R_{3z}^{-1}\mathbf{k})C_{3z}^{-1} = H(\mathbf{k}) \quad (2)$$

Here, R_{3z} is a threefold rotation acting on \mathbf{k} . Thus, the corresponding effective Hamiltonian, to the leading order, reads,

$$H = (C + \alpha k_z)\sigma_0 + v_z(k_z - k_w)\sigma_z + ak_- \sigma_+ + a^* k_+ \sigma_- \quad (3)$$

Here, C is the overall energy shift of bands. ‘ α ’ is the tilt term of spectrum, σ_0 is a 2×2 identical matrix, v_z is the Fermi velocity, σ ’s is the Pauli matrix, a is a parameter dependent of Fermi velocities in k_x - k_y , also indicating the anisotropic property in this plane

(corresponding to its complex value), and $k_{\pm} = k_x \pm ik_y$, $\sigma_{\pm} = \sigma_x \pm i\sigma_y$. This effective model indicates that the crossing point along H-K is a Weyl point, which is topologically protected, carrying ‘+1’ topological charge [62,63].

For this effective model, the corresponding eigenenergies are given by

$$\varepsilon_{\pm} = (C + \partial k_z) \pm \sqrt{v_z(k_z - k_w)^2 + |a|^2(k_x^2 + k_y^2)} \quad (4)$$

showing the linear dependence on \mathbf{k} . Here, \pm refers to the conduction and valance bands, respectively. One should note that, αk_z , which is linear to k_z tilts the cone-like spectrum in k_z direction, breaking the Lorentz invariance of Weyl fermions. Here, since the band structure shows a type-I-like Weyl point, $|\alpha| < v_z$. As a representative signature, WSMs can show Fermi arc in the surface band structure [4,10,13]. In Fig. 2(e), we display the (1 0 0) surface band structure of HfCuP. We indeed observe clear Fermi arc originating from the Weyl nodes in HfCuP.

Noticing that the states near the Fermi level in HfCuP mostly originate from the 5d orbitals of the heavy element Hf, they are expected to introduce pronounced SOC effect in the system. After taking into account SOC, the obtained band structure of HfCuP is shown in Fig. 3(a). Just as our expected, the band structure has changed much under SOC. On the one hand, under SOC all the bands are decoupled, because the system does not preserve inversion symmetry; on the other hand, the band splitting in the H-K path produces two Weyl nodes (denoted as W_1 and W_2), as shown in the enlarged band structure in Fig. 3(a). Very interestingly, we find W_1 and W_2 show different slops of band dispersions, where W_1 is a type-I Weyl node while W_2 is a type-II Weyl node. We have located the positions of all the Weyl nodes in the BZ, with W_1 at (0.333, 0.667, ± 0.125) and W_2 at (0.333, 0.667, ± 0.150). The positions of the Weyl nodes in the (1 0 0) surface are schematically shown in Fig. 3(b). From the lattice symmetry, there totally contain six pairs of type-I (W_1) and six pairs of type-II (W_2) Weyl nodes in HfCuP, locating at the H-K path in the BZ. We also calculated the surface band structure for HfCuP under SOC. As shown in Fig. 4 (c), from the (1 0 0) surface projection, we can observe two pieces of Fermi arcs originating from the two pairs of Weyl nodes in HfCuP.

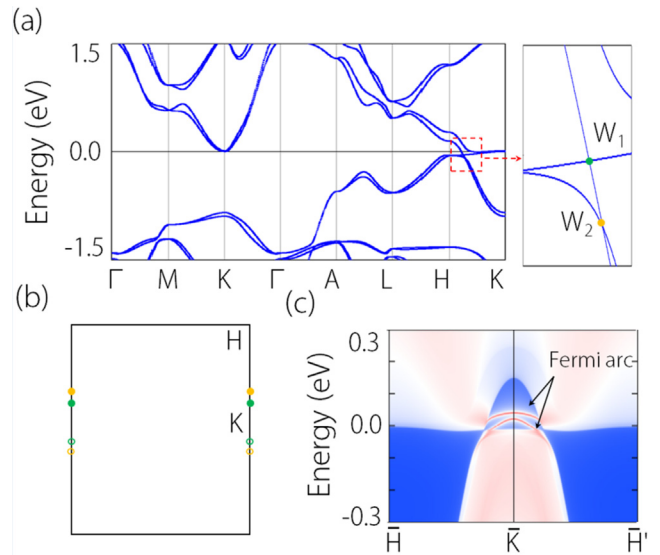


Fig. 3. (a) Electronic band structure of HfCuP with SOC included. The crossing points in the H-K path are denoted as W_1 and W_2 . (b) The positions of W_1 and W_2 in the (1 0 0) surface. In (b), the solid and hollow circles represent the “positive” and “negative” Weyl nodes. (c) The (1 0 0) surface band structure of HfCuP. In (c), the arrows point the Fermi arc surface states.

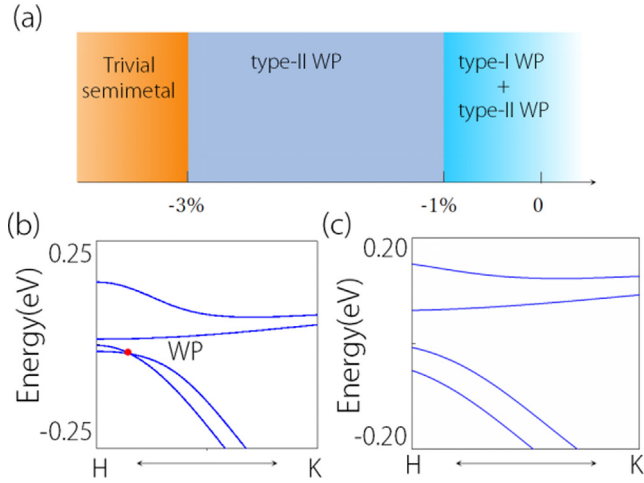


Fig. 4. (a) Topological phase diagram of HfCuP under biaxial strain in the a - b plane with SOC included. (b) Enlarged band structure of HfCuP along the H-K path under a 1% biaxial compressive strain. (c) Enlarged band structure of HfCuP along the H-K path under a 3% biaxial compressive strain. In (b) and (c), the band structures are calculated under SOC.

It is worth emphasizing that, HfCuP hosts type-I and type-II Weyl nodes simultaneously. This is quite different from previously identified WSMs, where the Weyl nodes with opposite chiralities have the same type of band dispersion. In addition, the Weyl nodes in HfCuP are quite suitable for experimental detection in that: first, all the Weyl nodes situate slightly below the Fermi level (where W_1 are at -40 meV and W_2 are at -88 meV); second, HfCuP has a very clean band structure that there nearly exists no extraneous bands near the Weyl nodes; third, HfCuP shows clear Fermi arc surface states from the Weyl nodes.

In the presence of SOC, there still exists a twofold degenerate point W_2 , the crossing bands can be chosen as the eigenstates of C_{3z} as well. Remarkably, the crossing bands belong to different 1D irreducible representations of the 156-symmetry group of H-K, such that they cannot hybridize each other. Consider basis states $|c_{3z}\rangle$ correspond to the $\{\Gamma_4, \Gamma_6\}$ of the eigenenergies $c_{3z} \in \{e^{-i\frac{2\pi}{3}}, -1\}$. These two eigenstates are mapped to each other by C_{3z} , such that $\{\Gamma_4, \Gamma_6\}$ gives a protected twofold degeneracy along this path. Specifically, the operator in the form of

$$C'_3 = \begin{bmatrix} -e^{-i\frac{2\pi}{3}} & 0 \\ 0 & -1 \end{bmatrix} \quad (5)$$

The effective Hamiltonian in this basis is in the form of

$$H = (C + \alpha k_z)\sigma_0 + v_z(k_z - k_w)\sigma_z + ak_- \sigma_+ + a^* k_+ \sigma_- \quad (6)$$

with $|\alpha| > v_z$, showing a type-II Weyl point.

In the space consisted by $\{\Gamma_4, \Gamma_5\}$ with $c_{3z} \in \{-e^{-i\frac{2\pi}{3}}, -e^{-i\frac{4\pi}{3}}\}$, these two 1D irreducible representations also contribute a double degenerate point W_1 . The three-fold rotation operation is given by

$$C''_3 = \begin{bmatrix} -e^{-i\frac{2\pi}{3}} & 0 \\ 0 & -e^{i\frac{2\pi}{3}} \end{bmatrix} \quad (7)$$

in the basis discussed above. Notably, the effective Hamiltonian reads,

$$H_{G_4, G_5} = (C + \alpha k_z)\sigma_0 + v_z(k_z - k_w)\sigma_z + ak_+ \sigma_+ + a^* k_- \sigma_- \quad (8)$$

This model also indicated a topologically protected Weyl point which carries an opposite topological charge as H_{G_4, G_6} . Here, one should note that the values for $\{C, v_z, a\}$ depend on the exactly model. It also results in a eigenenergies in the form of

$$\varepsilon_{\pm} = (C + \alpha k_z) \pm \sqrt{v_z^2(k_z - k_w)^2 + |a|^2(k_x^2 + k_y^2)} \quad (9)$$

Seeing from the band structure, one can get that $|\alpha| < v_z$.

Discussion, according to Bernevig's paper, "Type-II Weyl semimetals", the most general Hamiltonian describing the Weyl node is given by

$$H(k) = \sum_{ij} k_i v_{ij} \sigma_j \quad (10)$$

Here, $i = \{x, y, z\}$, $j = \{0, x, y, z\}$, σ 's is the Pauli matrix, v_{ij} is the coefficients.

For Eqs. (2), (4), and (9), the first term with α represents a tilt of spectrum, such that we have the energy spectrum:

$$E = (C + \alpha k_z) \pm \sqrt{v_z^2(k_z - k_w)^2 + a^2(k_x^2 + k_y^2)} \quad (11)$$

one can easily find the Weyl points locating at $(0, 0, k_w)$. Here, when α is small ($|\alpha| < |v_z|$), the spectrum shows a traditional band crossing for conventional Weyl node: The band crossing is linear, and the slopes of the crossing bands have opposite signs along k_z . On the other hand, when α is larger enough ($|\alpha| > |v_z|$) such that the tilt term dominates the spectrum. Then the spectrum is totally tipped over along $\text{sgn}(\alpha)k_z$, the two crossing bands have the same sign for their slopes. This feature is indicated in [Supplementary Information](#).

In addition, we find the band topology in HfCuP can be tuned by strain engineering. For example, by applying biaxial strain in the a - b plane, the type-I and type-II Weyl points can be annihilated sequentially. The corresponding phase diagram is shown in [Fig. 4](#) (a). Under the biaxial tensile strain, both the type-I and type-II Weyl points will retain. However, the band structure of HfCuP is quite sensitive to the biaxial compressive strain. A $\sim 1\%$ compressive strain will annihilate the type-I Weyl point, making HfCuP a pure type-II WSM. The representative band structure for this scenario is shown in [Fig. 4](#)(b). Under a larger compressive strain ($> 2.8\%$), the type-II Weyl point is also annihilated. As shown by the band structure in [Fig. 4](#)(c), there shows no band crossing in the H-K path, and HfCuP transforms from a WSM to a trivial semimetal under compressive strain larger than 2.8%. To be noted, in [Fig. 4](#)(a)–(c), SOC is included in the calculations. If SOC is omitted, HfCuP shows one pair of type-I Weyl nodes under biaxial tensile strains and compressive strains less than 4%. When the compressive strain is larger than 5%, the Weyl nodes will be gapped. The band structures under different strains without considering SOC are displayed in the [Supplementary Information](#). Therefore, strain can provide an effective method to control the Weyl nodes in HfCuP.

Summary

In summary, the electronic structure of HfCuP has been systematically studied by using first principles calculations. Without considering SOC, HfCuP shows six pairs of type-I Weyl nodes near the Fermi level in the H-K path, connected by clear Fermi Arcs. HfCuP experiences significant band splitting when SOC is taken into account. The band splitting in the H-K path produces twelve pairs of Weyl nodes, where six pairs are type-I and the others are type-II. The type-I Weyl nodes locate at $(0.333, 0.667, \pm 0.125)$ in the BZ, at -40 meV in energy. The type-II Weyl nodes situate at $(0.333, 0.667, \pm 0.150)$ in the BZ, at -88 meV in energy. The effective Hamiltonian has been constructed to describe the quasiparticle excitations near the Weyl nodes. Both the type-I and type-II Weyl nodes exhibit clear Fermi arc surface states. Moreover, we find the band topology in HfCuP can be tuned by strain engineering, so the Weyl nodes in HfCuP are controllable. Our results show that HfCuP

can provide a promising platform to explore the novel properties associated with type-I and type-II Weyl nodes.

Declaration of Competing Interest

The authors declare that they have no known competing financial interests or personal relationships that could have appeared to influence the work reported in this paper.

Acknowledgements

This work is supported by National Natural Science Foundation of China (Grants No. 11904074), Nature Science Foundation of Hebei Province (No. E2019202222), and the 333 Talent Project of Hebei Province (No. A2017002020). One of the authors (X.M. Zhang) acknowledges the financial support from Young Elite Scientists Sponsorship Program by Tianjin.

Compliance with ethics requirements

This article does not contain any studies with human or animal subjects.

Appendix A. Supplementary material

Supplementary data to this article can be found online at <https://doi.org/10.1016/j.jare.2020.05.026>.

References

- [1] Hasan MZ, Kane CL. Colloquium: Topological insulators. *Rev. Mod. Phys.* 2010;82:3045.
- [2] Qi X-L, Zhang S-C. Topological insulators and superconductors. *Rev. Mod. Phys.* 2011;83:1057.
- [3] Xu Y, Yan B, Zhang HJ, Wang J, Xu G, Tang P, et al. Large-gap quantum spin hall insulators in thin films. *Phys. Rev. Lett.* 2013;111:136804.
- [4] Wan X, Turner AM, Vishwanath A, Savrasov SY. Topological semimetal and Fermi-arc surface states in the electronic structure of pyrochlore iridates. *Phys. Rev. B* 2011;83:205101.
- [5] Burkov AA, Balents L. Weyl semimetal in a topological insulator multilayer. *Phys. Rev. Lett.* 2011;107:127205.
- [6] Young SM, Zaheer S, Teo JCY, Kane CL, Mele EJ, Rappe AM. Dirac semimetal in three dimensions. *Phys. Rev. Lett.* 2012;108:140405.
- [7] Zhao YX, Wang ZD. Topological classification and stability of Fermi surfaces. *Phys. Rev. Lett.* 2013;110:240404.
- [8] Wang Z, Weng H, Wu Q, Dai X, Fang Z. Three-dimensional Dirac semimetal and quantum transport in Cd_3As_2 . *Phys. Rev. B* 2013;88:125427.
- [9] Liu ZK, Zhou B, Zhang Y, Wang ZJ, Weng HM, Prabhakaran D, et al. Discovery of a three-dimensional topological Dirac semimetal, Na_3Bi . *Science* 2014;343:864.
- [10] Weng H, Fang C, Fang Z, Bernevig BA, Dai X. Weyl semimetal phase in noncentrosymmetric transition-metal monophosphides. *Phys. Rev. X* 2015;5:011029.
- [11] Chen C, Wang S-S, Liu L, Yu Z-M, Sheng X-L, Chen Z, et al. Ternary wurtzite CaAgBi materials family: A playground for essential and accidental, type-I and type-II Dirac fermions. *Phys. Rev. Mater.* 2017;1:044201.
- [12] Zhang XM, Guo RK, Jin L, Dai XF, Liu GD. Intermetallic Ca_3Pb : a topological zero-dimensional electride material. *J. Mater. Chem. C* 2018;6:575.
- [13] Lv BQ, Weng HM, Fu BB, Wang XP, Miao H, Ma J, et al. Experimental discovery of Weyl semimetal TaAs . *Phys. Rev. X* 2015;5:031013.
- [14] Weng H, Liang Y, Xu Q, Yu R, Fang Z, Dai X. Topological node-line semimetal in three-dimensional graphene networks. *Phys. Rev. B* 2015;92:045108.
- [15] Chen Y, Xie Y, Yang SA, Pan H, Zhang F, Cohen ML, et al. Nanostructured Carbon Allotropes with Weyl-like Loops and Points. *Nano Lett.* 2015;15:6974.
- [16] Fang C, Weng H, Dai X, Fang Z. Topological nodal line semimetals. *Phys. B* 2016;25:117106.
- [17] Liang Q-F, Zhou J, Yu R, Wang Z, Weng H. Node-surface and node-line fermions from nonsymmorphic lattice symmetries. *Phys. Rev. B* 2016;93:085427.
- [18] Wu W, Liu Y, Li S, Zhong C, Yu Z-M, Sheng X-L, et al. Nodal surface semimetals: Theory and material realization. *Phys. Rev. B* 2018;97:115125.
- [19] Zhang XM, Yu Z-M, Zhu ZM, Wu WK, Wang S-S, Sheng X-L, et al. Nodal loop and nodal surface states in the Ti_3Al family of materials. *Phys. Rev. B* 2018;97:235150.
- [20] Zhong C, Chen Y, Xie Y, Yang SA, Cohen ML, Zhang S. Towards three-dimensional Weyl-surface semimetals in graphene networks. *Nanoscale* 2016;8:7232.
- [21] Zhang J, Chan Y-H, Chiu C-K, Vergniory MG, Schoop LM, Schnyde AP. Topological band crossings in hexagonal materials. *Phys. Rev. Materials* 2018;2:074201.
- [22] Butcher Keith T, Gopalakrishnan Sai Gautam, Pieremanuele Canepa. *npj Comput. Mater.* 2019;5:4753.
- [23] Jin L, Zhang XM, He TL, Meng WZ, Dai XF, Liu GD. Topological nodal line state in superconducting NaAlSi compound. *J. Mater. Chem. C* 2019;7:10694–9.
- [24] Jin L, Zhang XM, Dai XF, Liu HY, Chen GF, Liu GD. Centrosymmetric Li_2NaN : a superior topological electronic material with critical-type triply degenerate nodal points. *J. Mater. Chem. C* 2019;7:1316–20.
- [25] Jin L, Zhang XM, Dai XF, Wang LY, Liu LY, Liu GD. Screening topological materials with a CsCl-type structure in crystallographic databases. *IUCr* 2019;6:2052–525.
- [26] Hou ZP, Wang WH, Wu GH, et al. Manipulating the topology of nanoscale skyrmion bubbles by spatially geometric confinement. *ACS Nano* 2019;13:922–9.
- [27] Hou ZP, Wang WH, Wu GH, et al. Creation of single chain of nanoscale skyrmion bubbles with record-high temperature stability in a geometrically confined nanostripe. *Nano Lett.* 2018;18:1274.
- [28] He TL, Zhang XM, Meng WZ, Jin L, Dai XF, Liu GD. Topological nodal lines and nodal points in the antiferromagnetic material $\beta\text{-Fe}_2\text{PO}_5$. *J. Mater. Chem. C* 2019;7:12657.
- [29] Liu PZ, James RW, Judy JC. Topological nanomaterials. *Nat. Rev. Mater.* 2019;4:479–96.
- [30] Yan BH, Felsner C. Topological materials: Weyl semimetals. *Annu. Rev. Condens. Matter Phys.* 2017;8:337–54.
- [31] Wu SG, Liu G, Li P, Liu H, Xu HH. A high-sensitive and fast-fabricated glucose biosensor based on Prussian blue/topological insulator Bi_2Se_3 hybrid film. *Biosens. Bioelectron.* 2012;38:289–94.
- [32] Xiao LP, Zhu AM, Xu QC, Chen Y, Xu J, Weng J. Colorimetric biosensor for detection of cancer biomarker by Au nanoparticle-decorated Bi_2Se_3 nanosheets. *ACS Appl. Mater. Interfaces* 2017;9:6931–40.
- [33] Politano A, Viti L, Vitiell MS. Optoelectronic devices, plasmonics, and photonics with topological insulators. *APL Mater.* 2017;5:035504.
- [34] Wang XT, Ding GQ, Cheng ZX, Surucu G, Wang XL, Yang T. Novel topological nodal lines and exotic drum-head-like surface states in synthesized CsCl-type binary alloy TiOs . *J. Adv. Res.* 2020;22:137–44.
- [35] Wang XT, Ding GQ, Cheng ZX, Surucu G, Wang XL, Yang T. Rich topological nodal line bulk states together with drum-head-like surface states in NaAlGe with anti-PbFCI type structure. *J. Adv. Res.* 2020;23:95–100.
- [36] Meng WZ, Zhang XM, He TL, Jin L, Dai XF, Liu GD. Crystal structures, electronic structures, and topological signatures in equiatomic $\text{TT}'\text{X}$ compounds ($\text{T} = \text{Sc, Zr, Hf}$; $\text{T}' = \text{Co, Pt, Pd, Ir, Rh}$; $\text{X} = \text{Al, Ga, Sn}$). *J. Phys. Chem. C* 2020;124:7378–85.
- [37] Jin L, Zhang XM, He TL, Meng WZ, Dai XF, Liu GD. Ferromagnetic two-dimensional metal-chlorides MCl ($\text{M} = \text{Sc, Y, and La}$): Candidates for Weyl nodal line semimetals with small spin-orbit coupling gaps. *Appl. Surf. Sci.* 2020;520:146376.
- [38] Ruan J, Jian SK, Yao H, Zhang H, Zhang SC, Xing D. Symmetry-protected ideal Weyl semimetal in HgTe -class materials. *Nat. Commun.* 2016;7:11136.
- [39] Ruan J, Jian SK, Zhang D, Yao H, Zhang H, Zhang S-C, et al. Ideal Weyl semimetals in the chalcopyrites CuTlSe_2 , AgTlTe_2 , and ZnPtAs_2 . *Phys. Rev. Lett.* 2016;116:226801.
- [40] Huang X, Zhao L, Long Y, Wang P, Chen D, Yang Z, et al. Observation of the chiral-anomaly-induced negative magnetoresistance in 3D Weyl semimetal TaAs . *Phys. Rev. X* 2015;5:031023.
- [41] Liu J, Vanderbilt D. Weyl semimetals from noncentrosymmetric topological insulators. *Phys. Rev. B* 2014;90:155316.
- [42] Hirayama M, Okugawa R, Ishibashi S, Murakami S, Miyake T. Weyl node and spin texture in trigonal tellurium and selenium. *Phys. Rev. Lett.* 2015;114:206401.
- [43] Son DT, Spivak BZ. Chiral anomaly and classical negative magnetoresistance of Weyl metals. *Phys. Rev. B* 2013;88:104412.
- [44] Liu C-X, Ye P, Qi X-L. Chiral gauge field and axial anomaly in a Weyl semimetal. *Phys. Rev. B* 2013;87:235306.
- [45] Huang SM, Xu SY, Belopolski I, Lee CC, Chang G, Wang B, et al. A Weyl Fermion semimetal with surface Fermi arcs in the transition metal monophosphide TaAs class. *Nat. Commun.* 2015;6:7373.
- [46] Xu SY, Belopolski I, Alidoust N, Neupane M, Bian G, Zhang C, et al. Discovery of a Weyl fermion semimetal and topological Fermi arcs. *Science* 2015;349:613.
- [47] Chang T-R, Xu S-Y, Chang G, Lee C-C, Huang S-M, Wang BG, et al. Prediction of an arc-tunable Weyl Fermion metallic state in $\text{Mo}_x\text{W}_{1-x}\text{Te}_2$. *Nat. Commun.* 2016;7:10639.
- [48] Soluyanov AA, Gresch D, Wang Z, Wu Q, Troyer M, Dai X, et al. Type-II Weyl semimetals. *Nature* 2015;527:495–8.
- [49] Chang T-R, Xu S-Y, Sanchez DS, Tsai W-F, Huang SM, Chang G, et al. Type-II symmetry-protected topological Dirac semimetals. *Phys. Rev. Lett.* 2017;119:026404.
- [50] Zyuzin AA, Tiwari RP. Intrinsic anomalous Hall effect in type-II Weyl semimetals. *JETP Lett.* 2016;103:717–22.
- [51] Koshino M. Cyclotron resonance of figure-of-eight orbits in a type-II Weyl semimetal. *Phys. Rev. B* 2016;94:035202.
- [52] O'Brien TE, Diez M, Beenakker CWJ. Magnetic breakdown and Klein tunneling in a type-II Weyl semimetal. *Phys. Rev. Lett.* 2016;116:236401.
- [53] Yu Z-M, Yao Y, Yang AS. Predicted unusual magnetoresistance in type-II Weyl semimetals. *Phys. Rev. Lett.* 2016;117:077202.

- [54] Chang G, Xu S-Y, Sanchez DS, Huang S-M, Lee C-C, Chang T-R, et al. A strongly robust type-II Weyl fermion semimetal state in Ta_3S_2 . *Sci. Adv.* 2016;2:e1600295.
- [55] Isobe H, Nagaosa N. Coulomb interaction effect in Weyl fermions with tilted energy dispersion in two dimensions. *Phys. Rev. Lett.* 2016;116:116803.
- [56] Li FY, Luo X, Dai X, Yu Y, Zhang F, Chen G. Hybrid weyl semimetal. *Phys. Rev. B* 2016;94:121105.
- [57] Wu YJ, Li HW, Jiang H, Xie XC. Global phase diagram of disordered type-II Weyl semimetals. *Phys. Rev. B* 2017;96.
- [58] Zhang MP, Yang Z, Wang GT. Coexistence of Type-I and Type-II Weyl points in the Weyl-semimetal OsC_2 . *J. Phys. Chem. C* 2018;122:3533–8.
- [59] Du XP, Wang YX. Investigation of osmium carbides with various stoichiometries: First-principles calculations. *J. Appl. Phys.* 2010;107:053506.
- [60] Szirtes L, Megyeri J, Riess L, Kuzmann E, Havancsak K. Swift heavy ion and gamma-ray irradiation of various double metal phosphates. *Radiat. Phys. Chem.* 2005;73:39–44.
- [61] Jain A, Ong SP, Hautier G, Chen W, Richards WD, Dacek S, et al. *APL Mater.* 2013;1:011002.
- [62] Chen F, Gilbert MJ, Dai X, Bernevig BA. Multi-Weyl topological semimetals stabilized by point group symmetry. *Phys. Rev. Lett.* 2012;108:266802.
- [63] Soluyano AA, Gresch D, Wang ZJ, Wu QS, Troyer M, Dai X, et al. Type-II weyl semimetals. *Nature* 2015;527:495–8.